Electronic Supplementary Material

Combined effects of sea urchin-like structure and mixed Cu^{+}/Cu^{0} states on promoting C_2 formation in electrocatalytic CO_2 reduction

Mengqing Shan, Dongsheng Lu, Jiatong Dong, Shen Yan, Jinyu Han, Hua Wang (✉)
Collaborative Innovation Center of Chemical Science and Engineering (Tianjin), Key Laboratory for Green Chemical Technology of the Ministry of Education, School of Chemical Engineering and Technology, Tianjin University, Tianjin 300354, China

E-mails: tjuwanghua@tju.edu.cn

Experimental characterization method

Lead Under Potential Deposition (Pb-UPD): Electrochemically active surface area (ECSA) analysis was performed to determine the ECSA of the catalysts by lead underpotential deposition in an electrolyte saturated with N_2 of 0.1 M $HClO_4$ and 1 mM $PbCl_2$ solution. The samples were subjected to cyclic Voltammetry (CV) sweeps in the range of -0.4 V to -0.7 V *vs.* RHE with a sweep rate of 10 mV/s.

OH^- adsorption spectra by CV: In order to characterize the surface structure of the catalyst, the OH^- adsorption on the catalyst surface was examined by CV test. The CV test for OH^- adsorption was carried out in N_2 saturated solution of 0.1 M KOH at a scanning rate of 10 mV/s.

Infrared detection of CO adsorption: The samples were pretreated with He gas at 473 K for 2 h at a flow rate of 40 mL min^{-1}. The CO adsorption process was carried out by passing CO gas after waiting for the temperature to drop to room temperature, and the adsorption was saturated and purged with He. The CO adsorption after adsorption saturation and at the end of the purge were compared to evaluate the CO adsorption amount and adsorption strength of the catalyst.

CO temperature-programmed desorption (CO-TPD): The 200 mg catalyst was pretreated at 473 K for 2 h with He gas at a flow rate of 40 mL min^{-1}. Subsequently, the CO adsorption process was performed at 278 K by injection of a mixture of CO + He (5% CO) and the desorbed CO was measured by a thermal conductivity detector (TCD) with a mass spectrometer while the temperature was ramped from 278 K to 800 K with an acceleration of 5 K min^{-1}.

Electrocatalytic CO_2 reduction tests

Working Electrode Preparation:

For H-cell: 5 mg CuO/Cu_2O particles and 50 μL 5% Nafion were dispersed in 250 μL deionized water and 200 μL methanol, then ultrasonicated for 20 min to homogeneously disperse the catalyst, and then 100 μL of ink was dropped onto 1 × 1 cm^2 hydrophobic carbon paper in five batches and allowed to dry naturally. The working electrode procedure for Cu_2O particles was as above.

For flow cell: 10 mg CuO/Cu_2O particles and 100 μL 5% Nafion were dispersed in 100 μL deionized water and 800 μL methanol, then ultrasonicated for 20 min to homogeneously disperse the catalyst, and then 200 μL of ink was dropped onto 1.5 cm × 1.4 cm hydrophobic carbon paper in five batches and allowed to dry naturally.

Electrocatalytic CO_2 performance:

H-cell: The tests were carried out in a typical H-type electrolytic cell divided by a Nafion 211 membrane, and electrochemical reactions were recorded using a CHI660e electrochemical workstation.

A typical three-electrode system was used, with a platinum foil (1 cm × 1 cm) and an Ag/AgCl electrode (saturated KCl solution) as counter and reference electrodes, respectively. The area of the working electrode was fixed at 1 cm^2. The measured potentials were calibrated to RHE according to the following method:

$$V_{RHE} = V_{Ag/AgCl} + 0.197 + 0.059\ V \times pH$$

Prior to CO_2RR, the cathode and anode were each injected with 30 mL of 0.1 M $KHCO_3$ solution, and then high-purity CO_2 (99.999%) was bubbled into the cathode chamber electrolyte for 30 min, and then pre-reduction treatment was performed at -0.54 V *vs.* RHE 20 min, with the CO_2 gas flow rate of 50 mL/min (sccm). The electrolysis test was then performed at a fixed potential for 1 h, with the CO_2 gas flow rate of 20 sccm, accumulating enough product for accurate testing.

Flow cell: A three-electrode, three-compartment device was used in the flow cell operation. A catalyst-loaded gas diffusion electrode (GDE) was used as the working electrode, while nickel foam and Ag/AgCl electrode (saturated KCl solution) were used as the counter electrode and reference electrode, respectively. The cathode and anode chambers are separated by an anion exchange membrane (FAA-3-50). The cathode liquid flow rate was 8 mL min^{-1}. The CO_2 gas flow rate was 20 sccm and flowed through the back of the GDE. Connected to an on-line chromatograph, the gas product was detected at regular intervals and the liquid product was collected at the end of the reaction and tested by 600 M 1hydrogen-nuclear magnetic resonance (600 M ^{1}H-NMR).

Product Analysis

Analysis of products during electrolysis using on-line gas chromatography. H_2 was detected by a thermal conductivity detector (TCD) and CO, CH_4, C_2H_4, C_2H_6 were detected by a flame ionization detector (FID). After electrolysis, 520 μL of electrolyte, 100 μL of D_2O and 30 μL of internal standard DMSO were mixed and the liquid products HCOOH, C_2H_5OH were analyzed by 600 M ^{1}H-NMR. The Faraday efficiency of each product was calculated using the following equation:

$$FE(\%) = nzF/Q \times 100\%$$

Where F is the Faraday constant, n is the number of electrons required to produce one molecule of the product, z is the molar amount of the product and Q is the total charge through the working electrode.

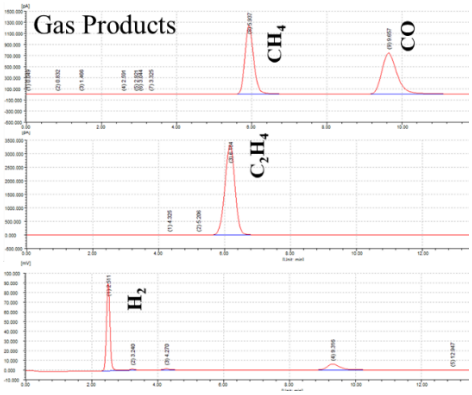

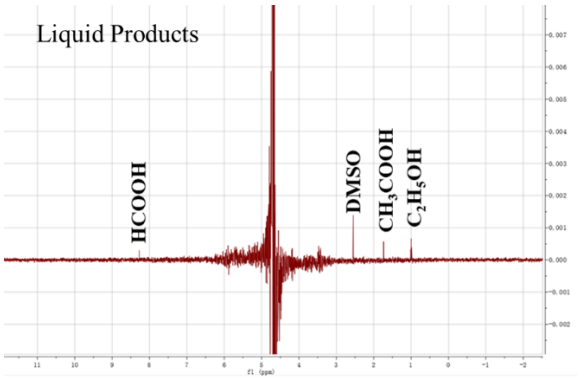

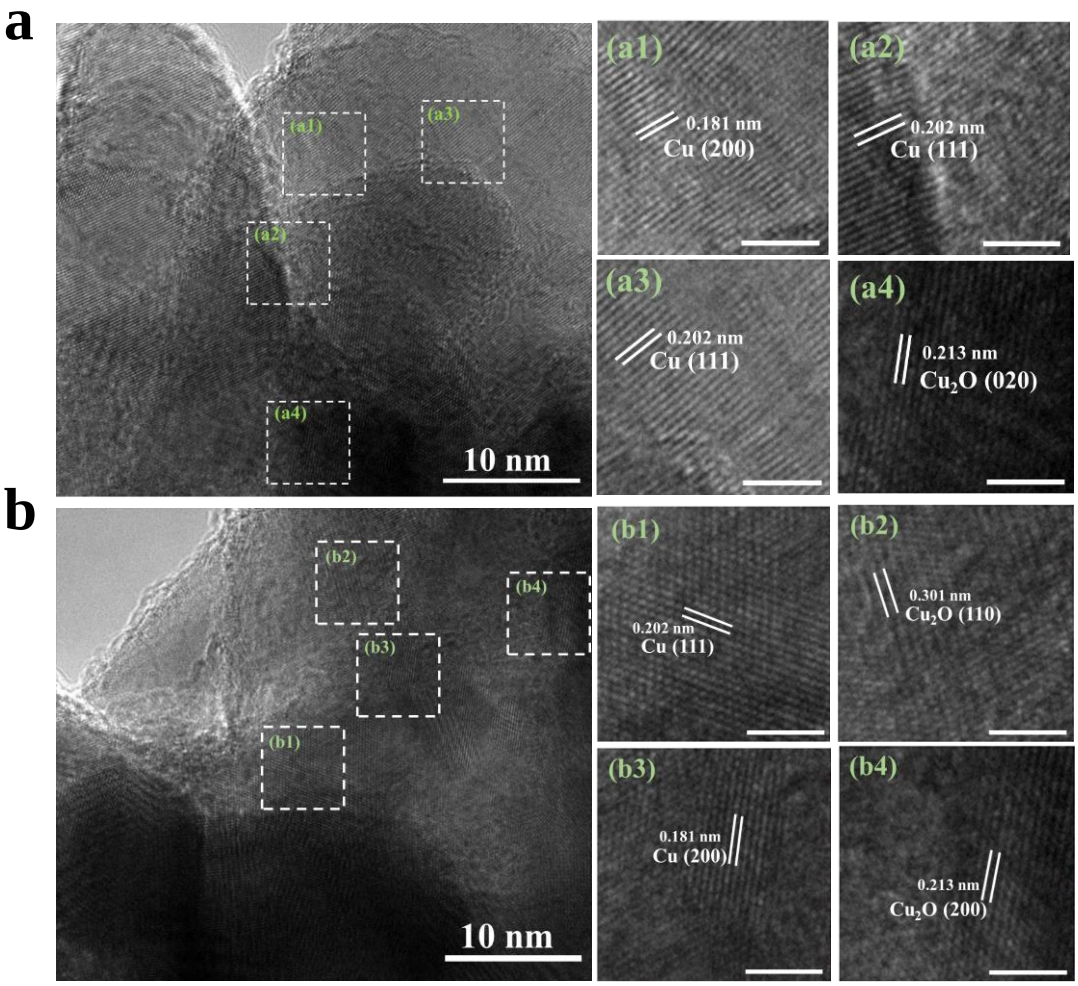

Fig. S1 (a, b) HRTEM images of R-CuO/Cu_2O nanoparticles after electrolysis at -1.4 V *vs.* RHE. The bars represent 3 nm for (a1-a4) and (b1-b4).

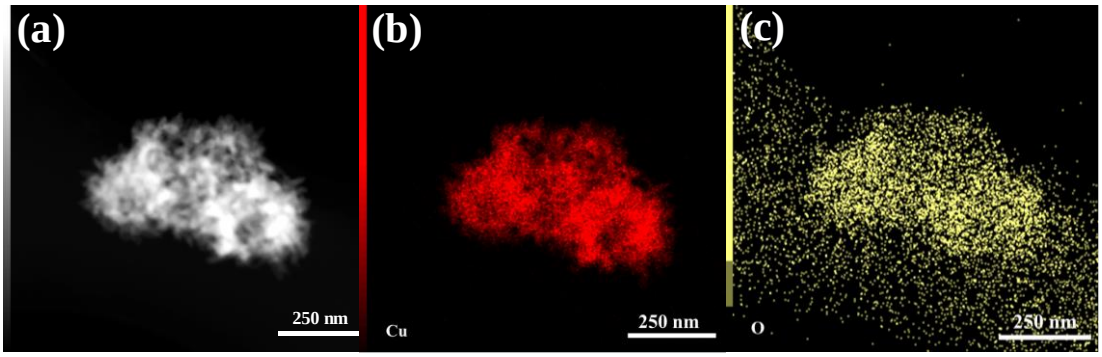

Fig. S2 (a) STEM images of R-CuO/Cu_2O. (b-c) The elemental mapping of the elements Cu and O.

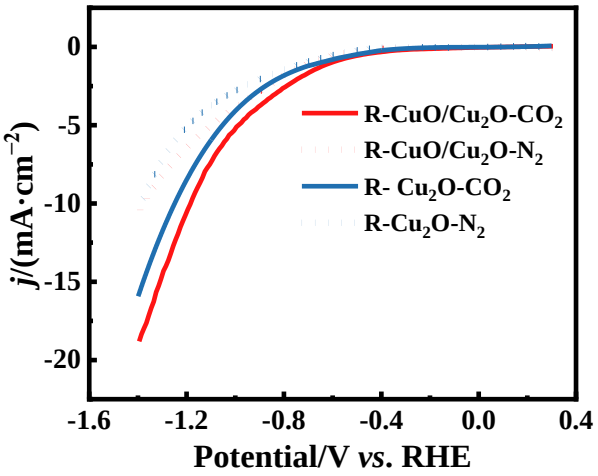

Fig. S3 LSV curves of R-Cu_2O and R-CuO/Cu_2O catalysts in 0.1 M $KHCO_3$ saturated with N_2 and CO_2, respectively.

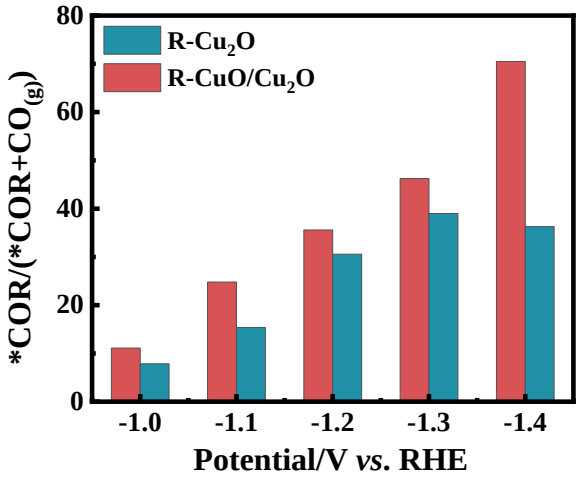

Fig. S4 *COR/(*COR+CO(g)) for R-Cu_2O and R-CuO/Cu_2O at different potentials.

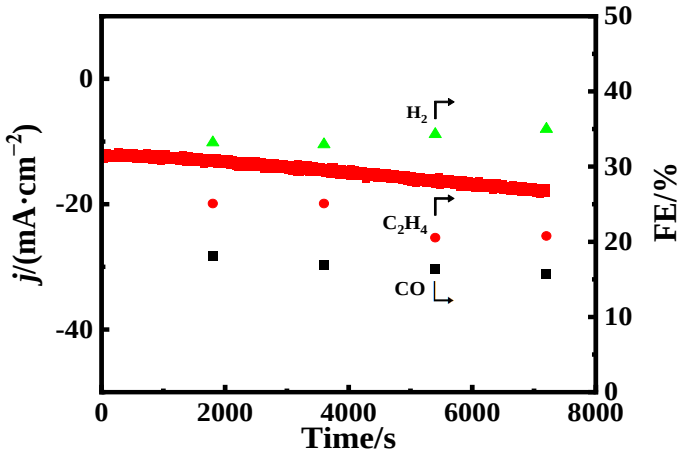

Fig. S5 I-t curve and FEs of H_2, C_2H_4 and CO on R-Cu_2O catalyst at -1.4 V *vs.* RHE.

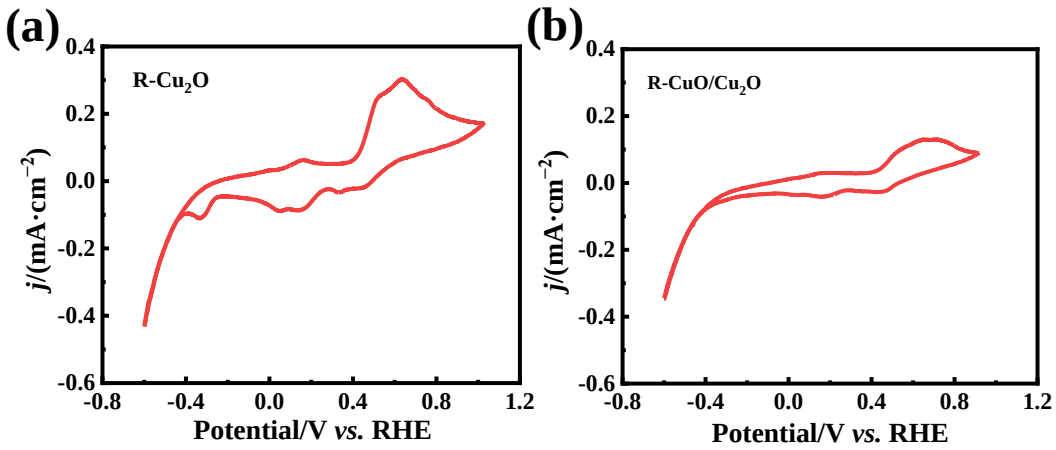

Fig. S6 (a, b) CV curves of R-Cu_2O and R-CuO/Cu_2O after electrolysis.

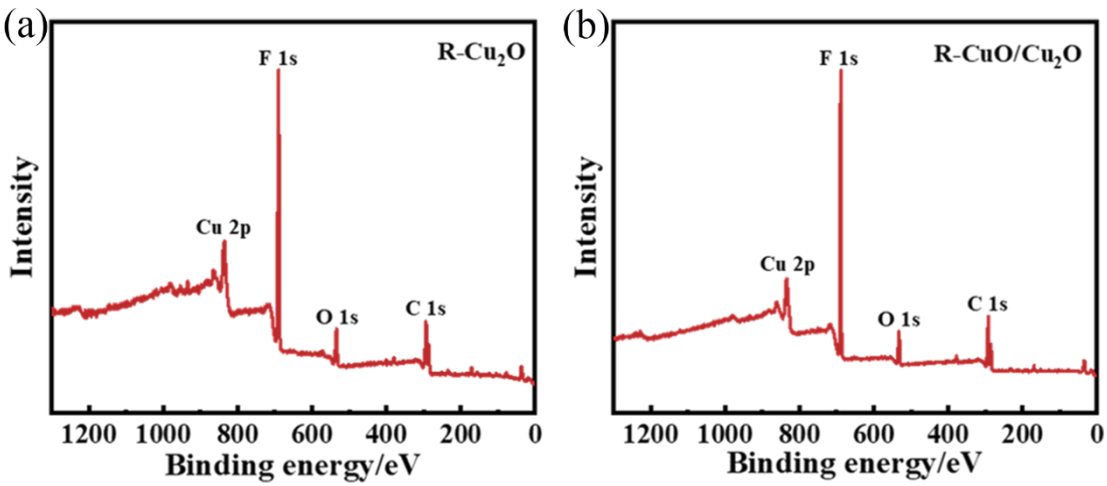

Fig. S7 The XPS survey spectra of (a) R-Cu_2O and (b) R-CuO/Cu_2O.

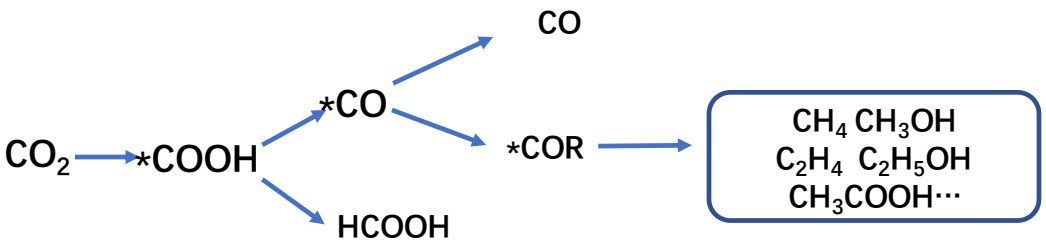

Scheme S1 Conversion of key intermediates in the CO_2RR.

Table. S1 Performance comparison of the reported Cu-based electrocatalysts for CO_2RR to C_{2+} products under comparable conditions.

Catalyst	Reactor	Electrolyte	FE_{C2+} (%)	J_{C2+} (mA cm^{-2})	Ref.
$Cu/C_{6.6}$	Flow cell	1.0 M KOH	63.2	505.6	[1]
$CuO\text{-}C_{60}$	Flow cell	1.0 M KOH	61.0	366.0	[2]
CuO/Cu_2O	Flow cell	1.0 M $KHCO_3$	68.0	340.0	This work
Cu_{500} CL	Flow cell	1.0 M KOH	79.0	316.0	[3]
M-Cu_1/CuNP	Flow cell	5.0 M KOH	75.4	289.2	[4]
F-doped Cu	Flow cell	1.0 M KOH	70.4	281.6	[5]
Cu needles	Flow cell	1.0 M KOH	64.0	255.0	[6]
Fragmented Copper	Flow cell	7.0 M KOH	77.8	233.4	[7]
Cu_4O_3-rich	Flow cell	0.5 M Cs_2SO_4	61.0	200.0	[8]
Cu_2O nanocube	Flow cell	1.0 M KOH	61.1	152.8	[9]
Cu(salophen)-coated	Flow cell	1.0 M KOH	40.0	124.0	[10]
$Cu_{1.4}$Ni SAC	Flow cell	0.1 M $KHCO_3$	91.0	90.0	[11]

References

1. Kong X, Wang C, Xu Z, Zhong Y, Liu Y, Qin L, Zeng J, Geng Z. Enhancing CO_2 electroreduction selectivity toward multicarbon products via tuning the local H_2O/CO_2 molar ratio. Nano Letters, 2022, 22(19): 8000-8007
2. Zhao B, Chen F, Cheng C, Li L, Liu C, Zhang B. C_{60}-Stabilized Cu^+ sites boost electrocatalytic reduction of CO_2 to C_{2+} products. Advanced Energy Materials, 2023, 13(19): 2204346.
3. Wang X, Chen Q, Zhou Y, Tan Y, Wang Y, Li H, Chen Y, Sayed M, Geioushy R A, Allam N K, et al. Gas diffusion in catalyst layer of flow cell for CO_2 electroreduction toward C_{2+} products. Nano Research, 2023: 1-6
4. Feng J, Zhang L, Liu S, Xu L, Ma X, Tan X, Wu L, Qian Q, Wu T, Zhang J, et al. Modulating adsorbed hydrogen drives electrochemical CO_2-to-C_2 products. Nature Communications, 2023, 14(1): 4615
5. Yan X, Chen C, Wu Y, Chen Y, Zhang J, Feng R, Zhang J, Han B. Boosting CO_2 electroreduction to C_{2+} products on fluorine-doped copper. Green Chemistry, 2022, 24(5): 1989-1994
6. Sun R, Wei C, Huang Z, Niu S, Han X, Chen C, Wang H, Song J, Yi J-D, Wu G, et al. $Cu_{2+1}O/CuO_x$ heterostructures promote the electrosynthesis of C_{2+} products from CO_2. Nano Research, 2022, 16(4): 4698-4705
7. Yao K, Li J, Wang H, Lu R, Yang X, Luo M, Wang N, Wang Z, Liu C, Jing T, et al. Mechanistic insights into OC–COH coupling in CO_2 electroreduction on fragmented copper. Journal of the American Chemical Society, 2022, 144(31): 14005-14011
8. Martić N, Reller C, Macauley C, Löffler M, Schmid B, Reinisch D, Volkova E, Maltenberger A, Rucki A, Mayrhofer K J J, et al. Paramelaconite-enriched copper-based material as an

efficient and robust catalyst for electrochemical carbon dioxide reduction. Advanced Energy Materials, 2019, 9(29): 1901228

9. Jeon H S, Timoshenko J, Rettenmaier C, Herzog A, Yoon A, Chee S W, Oener S, Hejral U, Haase F T, Roldan Cuenya B. Selectivity control of Cu nanocrystals in a gas-fed flow cell through CO_2 pulsed electroreduction. Journal of the American Chemical Society, 2021, 143(19): 7578-7587
10. Zhu L-J, Si D-H, Ma F-X, Sun M-J, Zhang T, Cao R. Copper–supramolecular pair catalyst promoting C_{2+} product formation in electrochemical CO_2 reduction. ACS Catalysis, 2023, 13(8): 5114-5121
11. Li S, Guan A, Yang C, Peng C, Lv X, Ji Y, Quan Y, Wang Q, Zhang L, Zheng G. Dual-atomic Cu sites for electrocatalytic CO reduction to C_{2+} products. ACS Materials Letters, 2021, 3(12): 1729-1737